Hindawi
Mathematical Problems in Engineering
Volume 2022, Article ID 4934723, 13 pages
https://doi.org/10.1155/2022/4934723

Research Article

Coordinated Vehicle Lateral Stability Control Based on Direct Yaw Moment and Engine Torque Regulation under Complicated Road Conditions

Liu Gang [1,2] **and Qiao Lin-Yan** [1]

[1]*Department of Automotive Engineering, Henan Institute of Technology, Xinxiang 453000, China*
[2]*XinXiang Research Center of Automobile Chassis Control and Auxiliary Safety Engineering, Xinxiang 453000, China*

Correspondence should be addressed to Liu Gang; 79046248@qq.com

Received 17 August 2022; Revised 3 October 2022; Accepted 15 October 2022; Published 28 October 2022

Academic Editor: Shangce Gao

This paper proposed a control method of vehicle lateral stability control system. In order to obtain the best driving performance under the complicated friction conditions track, the direct yaw moment (DYC) and the engine torque regulation (ETC) value need to be adjusted to avoid penalisation of each other. Firstly, the intervention timing of direct yaw moment control and engine torque regulation control is studied, which is judged by the phase plane method and longitudinal speed threshold method, respectively. Then, a direct yaw moment control algorithm based on sliding mode control algorithm is designed, and its target value calculation depends on the linear two-degree-of-freedom model. The engine torque regulation is calculated by fuzzy algorithm. The input values are mainly the vehicle state parameters and the driver's input to the steering wheel. Matlab/Simulink, AMESim, and CarSim software programs are used to simulate sine with dwell maneuver. The simulation results show the effectiveness of the cooperation control algorithm proposed in this paper.

1. Introduction

Vehicle handling stability is an important performance evaluation factor for the vehicle [1, 2]. Handling stability can effectively avoid accidents. At present, direct yaw moment control is a well-known vehicle stability control method and has been widely used. DYC collects steering wheel angle information and vehicle motion status information through sensors. The driver's driving intention is calculated according to the sensor data. Direct yaw moment control is used to adjust the yaw motion of the vehicle. The direct yaw moment is obtained by applying different wheel forces (driving or braking forces) between the inner and outer wheels [3–5].

Many scholars have published a lot of studies on ESC control. In reference [6], PI (proportional integral) feedback control is used to improve the lateral stability of electric vehicles by controlling the distribution of driving torque between wheels. However, under some complex conditions, such as low adhesion coefficient road condition, PI control cannot achieve satisfactory results. Then, in reference [3], neural network PID algorithm is used to enhance vehicle lateral stability and maneuverability. Although the above neural PID control strategies partially improve the system performance, they are also not suitable for extreme working conditions. In order to solve the problem of poor vehicle stability under extreme conditions, some nonlinear control algorithms are also applied to DYC, such as nonsmooth control [7], fuzzy control [8], optimal control [9], H ∞ controls [10, 11], and so on [5, 12–15].

The sideslip angle-sideslip angular velocity phase plane is established as the stability criterion. Based on the sideslip angle-sideslip angular velocity phase plane, the driving system dynamics will enter a highly nonlinear regime when the curve exceeds a certain stability threshold. Therefore, the robust controller is suitable to deal with this nonlinear

problem. In particular, the sliding mode control method has been widely studied in recent years because of its simple algorithm and is suitable for nonlinear systems [16]. The sliding mode control method has been widely studied in recent years. On the one hand, the sliding mode control method effectively rejects the uncertainties [17–19]. On the other hand, the algorithm is simple and has fast response [20, 21]. Hence, it is obvious that the SMC method is a very effective tool for lateral stability control [22, 23]. Tohru Yoshioka applied sliding mode theory to direct yaw moment control [4]. In [24], the SM observers are applied to estimate the vehicle sideslip angle. The second-order sliding mode controller is further developed for the sake of driving the vehicle sideslip angle to their reference signals.

Engine torque control is also one of the core research issues in the field of vehicle dynamics control. In [25], model predictive control is used to adjust engine output torque. In [26], adaptive sliding mode control is applied to the process of traction control.

The above methods emphasize on the DYC. However, under extremely complicated condition, it is very important to coordinate the engine torque control and the DYC to guarantee the stability of vehicle. Unfortunately, two control methods may interfere with each other. Therefore, it is necessary to design a method that uses these two controllers.

This paper presents a coordinated method based on the ETC and DYC. This method is designed with the idea of hierarchical control, as shown in Figure 1. The state variables of the vehicle, such as sideslip angle, longitudinal acceleration, lateral acceleration, and wheel speed, can be estimated by the observer or collected by the sensor. The upper controller mainly includes three parts: vehicle stability state judgment, target value calculation, and stability control algorithm. The direct yaw moment is calculated by the DYC module in the upper controller and sent to the lower controller. The target braking pressure is calculated by the lower controller based on the direct yaw moment. The target braking pressure is processed by the wheel cylinder pressure control module and sent to the hydraulic execution unit, which is responsible for braking. The engine torque regulation value is calculated by the ETC module and sent to the engine management unit. In the software simulation and vehicle test, three simulation conditions are used to verify the effectiveness of the coordinated control strategy of DYC and ETC. The following conclusions can be drawn: by using a joint control method, the peak value of the yaw rate for joint control decreases significantly, indicating improved stability.

The paper is organised as follows. Section 2 presents the control intervention judgment and the coordinated control strategy. Section 3 proposes the algorithm of DYC. Section 4 discusses the algorithm of ETC. Section 5 reports the simulation results. Section 6 reports the experiment results. Finally, Section 7 presents the conclusions.

2. Control Intervention Judgment of DYC and ETC

2.1. Judgment of Intervention Time of DYC Control. According to the driver's steering wheel input signal and vehicle state parameters, the ESC system judges the vehicle stability and determines whether ESC control intervention is needed. The timing of DYC intervention was mainly based on the phase plane method. The boundary of whether the vehicle is in stable or unstable state is generally represented by two lines symmetrical about the origin in the phase plane [27]. For the phase plane method, the linear model of the vehicle stability boundary is as follows [28–30]:

$$\left|B_1\dot{\beta}+\beta\right| \le B_2, \tag{1}$$

where B_1 and B_2 represent the regulating variable and the boundary variable, respectively. By changing the values of B_1 and B_1 variables, the vehicle state can be divided into stable state and unstable state, and the unstable state needs to be controlled by DYC. β is the sideslip angle. As the road adhesion coefficient will affect the judgment of vehicle stability, the values of B_1 and B_2 vary according to the road adhesion coefficient, as shown in Table 1.

As shown in Figure 2, when the vehicle is in a stable state, the change trend of yaw rate and sideslip angle closely follows the driver's input signal, and DYC will not intervene in the control at this time. However, when the vehicle state parameters enter the unstable state as shown in Figure 2, DYC intervention is needed to ensure the lateral stability of the vehicle. The flowchart of DYC intervention timing judgment is shown in Figure 3.

2.2. Judgment of Intervention Time of ETC. When the vehicle is turning, the relationship among lateral acceleration, longitudinal speed, and yaw rate can be expressed as follows:

$$a_y = \dot{v}_y + v_x\dot{\varphi}, \tag{2}$$

where a_y is the lateral acceleration; v_x is the longitudinal speed; $\dot{v}_y$ is the differential of the lateral speed; and $\dot{\varphi}$ is the yaw rate. When the vehicle is in a stable state, the lateral acceleration of the vehicle is less than the maximum acceleration provided by the road adhesion. In a short time (less than 10 ms), the change rate of longitudinal speed and lateral speed is about 0, and the reference value of vehicle lateral acceleration in steady state is as follows:

$$a_{y\_\mathrm{ref}} = \left|v_x\dot{\varphi}\right| = \left|\frac{\delta v_x^2}{L\left(1+Kv_x^2\right)}\right|, \tag{3}$$

where δ is the front wheel angle parameter; L is the distance from front axle to rear axle; and K is the stability parameter; when the formula $1+Kv_x^2<0$ is true, it means that the vehicle is unstable.

The maximum lateral acceleration provided by road adhesion is as follows [18]:

$$a_{y\_\max} = \mu_{\max} g, \tag{4}$$

where $\mu_{\max}$ is the maximum value of the road adhesion coefficient and g is the acceleration of gravity.

In this paper, the ratio of a_{y_ref} to $a_{y\_\max}$ is taken as the state coefficient of vehicle stability:

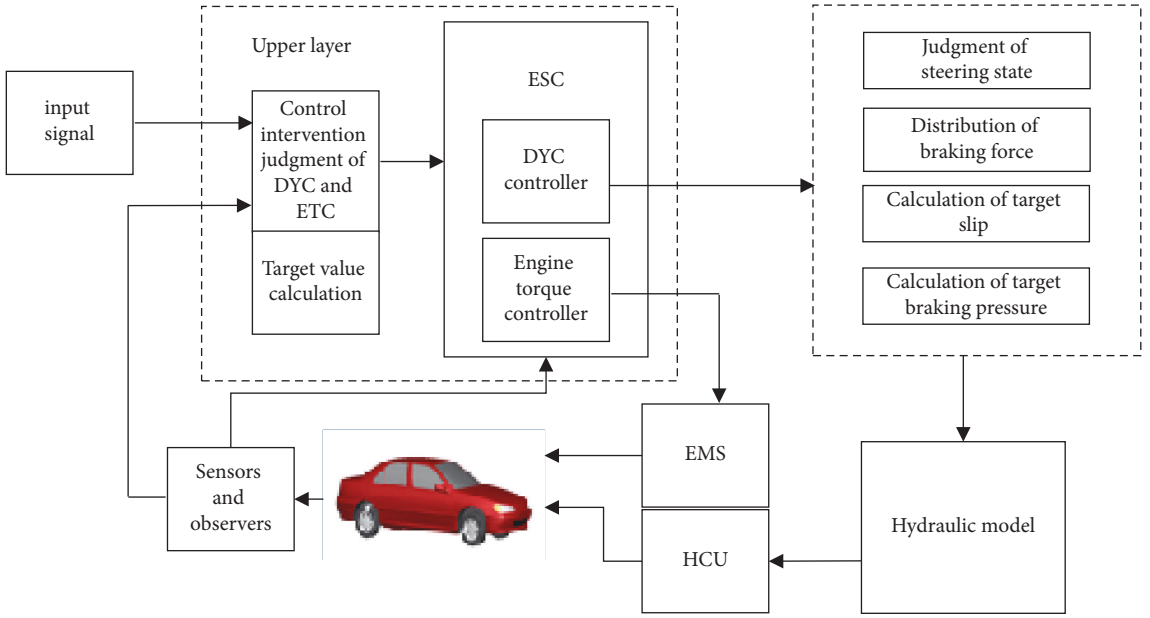

Figure 1: The controller structure for ESP.

Table 1: The values of B_1 and B_2.

Road adhesion coefficient	B_1	B_2
$0.8 \le \mu < 1$	0.35	5.57
$0.6 \le \mu < 0.8$	0.33	4.65
$0.4 \le \mu < 0.6$	0.3	4.22
$0.2 \le \mu < 0.4$	0.29	3.34
$\mu < 0.2$	0.28	2.57

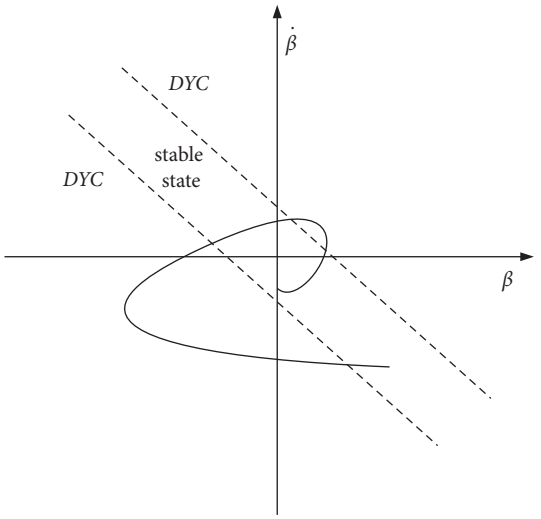

Figure 2: Schematic diagram of DYC intervention timing.

$$K_{\text{factor}} = \frac{a_{y\_\text{ref}}}{a_{y\_\max}} = \frac{|\delta| v_x^2}{L\left(1 + K v_x^2\right)\mu g} = \frac{|\delta|}{L\left(\left(1/v_x^2\right) + K\right)\mu g}. \quad (5)$$

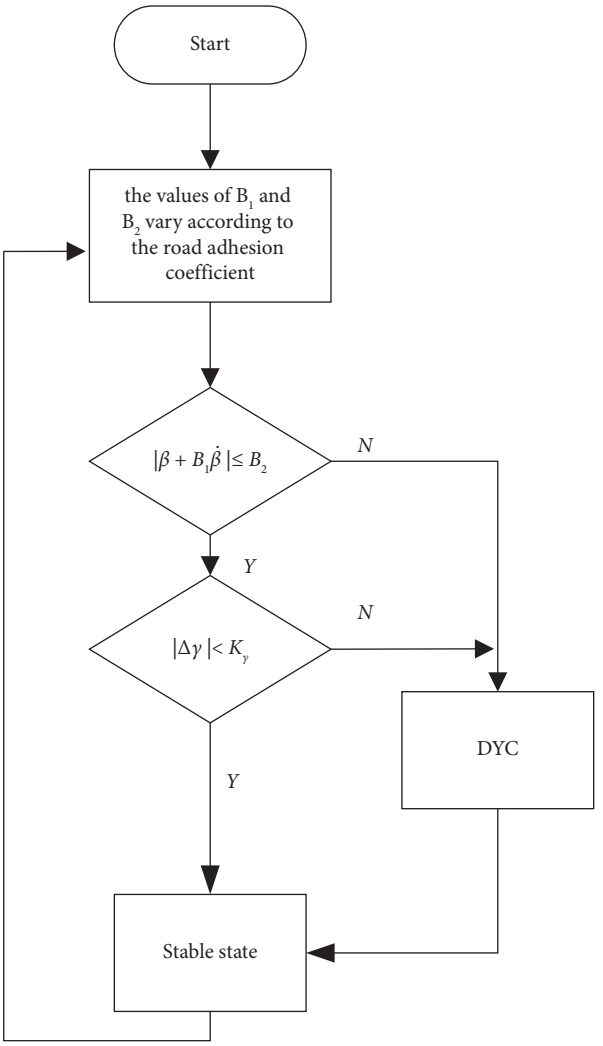

Figure 3: Flowchart of DYC intervention timing judgment.

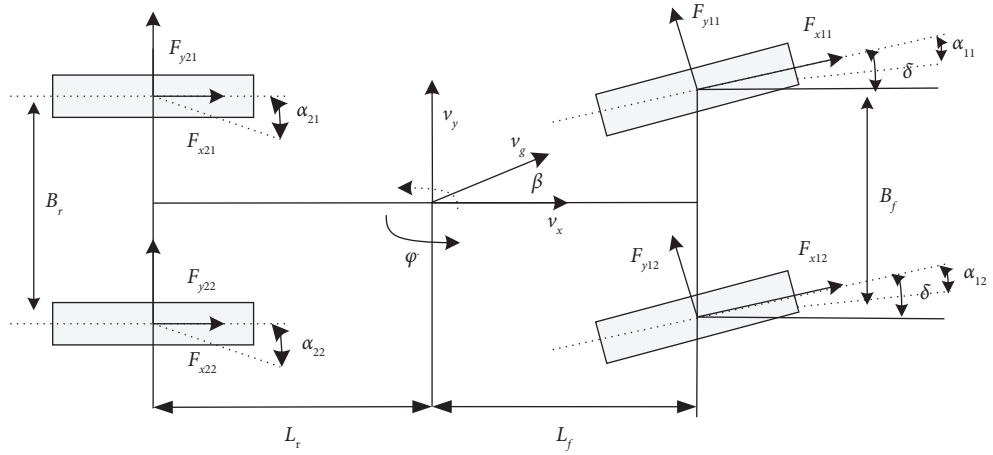

Figure 4: 3-DOF nonlinear vehicle model.

The stability state parameter K_{factor} represents the degree of the vehicle's stability state. When the road adhesion coefficient has been determined, the increase of K_{factor} indicates that the lateral acceleration approaches or exceeds the limit value of the lateral acceleration provided by the road, and the vehicle may be in an unstable state at the next moment; the decrease of K_{factor} indicates that the vehicle is gradually approaching a stable state. Therefore, the threshold A_s is set in this article. When $K_{\text{factor}} <= A_s$, it means that the vehicle is laterally stable. Analyzing (5), it can be seen that when the road surface coefficient is a fixed value, the vehicle reduces the longitudinal speed to ensure the lateral stability of the vehicle when turning. The threshold of longitudinal vehicle speed when the vehicle is turning can be obtained:

$$v_{x\_\text{limit}} = \sqrt{\frac{K_{\text{factor}}\mu g L}{\delta_{\text{last}} - K \cdot K_{\text{factor}}\mu g L}}, \tag{6}$$

where δ_{last} represents the front wheel angle parameter at the previous moment.

When the car is turning, the longitudinal speed exceeds v_{x_limit}, which means that the side force provided by the current road surface is less than the side force required to maintain the stability of the vehicle. The vehicle is gradually unable to maintain stability. Therefore, it is necessary to rely on the ETC module to reduce the engine output torque according to the current vehicle state parameters and road conditions, so as to reduce the longitudinal speed of the vehicle and maintain the lateral stability of the vehicle.

3. Direct Yaw Moment Control Algorithm

The control variables of DYC are the yaw rate and the center of mass slip angle. The yaw rate can accurately describe the rotation of the vehicle during turning. The center of mass slip angle reflects the deviation of the vehicle from the driving track during the steering process. The calculation of the target value of the yaw rate and the side slip angle of the center of mass is available in reference [31].

The vehicle model adopts a 3-degree-of-freedom model, which can accurately describe the mathematical relationship between longitudinal force, lateral force, and yaw moment during the turning process [32], as shown in Figure 4, and the expression is

$$\begin{cases} m\left(\dot{v}_x - v_y\dot{\varphi}\right) = \sum_{i,j=1}^{2} F_{xij} = \left(F_{x11} + F_{x12}\right)\cos\delta + \left(F_{x21} + F_{x22}\right) - \left(F_{x11} + F_{x12}\right)\sin\delta, \\ m\left(\dot{v}_y + v_x\dot{\varphi}\right) = \sum_{i,j=1}^{2} F_{yij} = \left(F_{y11} + F_{y12}\right)\cos\delta + \left(F_{y21} + F_{y22}\right) - \left(F_{y11} + F_{y12}\right)\sin\delta, \\ I_{zz}\ddot{\varphi} = M_z = \left(F_{y11}\cos\delta + F_{x11}\sin\delta + F_{x12}\sin\delta + F_{y12}\cos\delta\right)L_f \\ \quad - \left(F_{x12}\cos\delta - F_{y12}\sin\delta - F_{x11}\cos\delta + F_{y11}\sin\delta\right)\frac{B_f}{2} \\ \quad - L_r\left(F_{y21} + F_{y22}\right) + \frac{B_r}{2}\left(F_{x21} - F_{x22}\right), \end{cases} \tag{7}$$

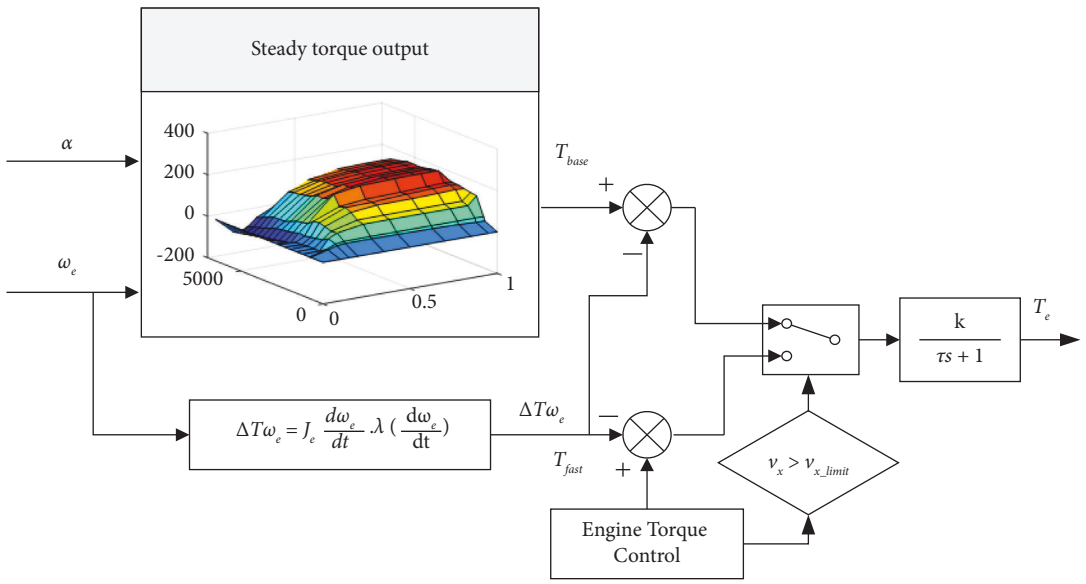

Figure 5: Architecture of engine torque control algorithm.

where F_{x11} is the tire longitudinal force of the left front wheel of the vehicle; F_{x12} is the tire longitudinal force of the right front wheel of the vehicle; F_{x21} is the tire longitudinal force of the left rear wheel of the vehicle; F_{x22} is the tire longitudinal force of the right rear wheel of the vehicle; $\sum_{i,j=1}^{2} F_{xij}$ is the sum of the longitudinal forces; F_{y11} is the tire lateral force of the left front wheel of the car; F_{y12} is the tire lateral force of the right front wheel of the car; F_{x21} is the tire lateral force of the left rear wheel of the car; F_{x22} is the tire lateral force of the right rear wheel of the car; $\sum_{i,j=1}^{2} F_{yij}$ is the sum of the lateral forces of the four wheels; $\sum M_z$ is the yaw moment of the car; v_g is the speed of the center of mass of the car; a_x is the lateral acceleration at the center of mass of the car; m is the total mass of the vehicle; I_{zz} is the moment of inertia of the vehicle in the z-axis direction; I_{xxs} is the moment of inertia of the x-axis; L_f is the distance from the front axle of the vehicle to the center of mass; L_r is the distance from the rear axle of the vehicle to the center of mass; B_f is the distance between the two front wheels; and B_f is the distance between the two rear wheels.

The front wheel sideslip angle δ of a car is very small, so its sine value can be considered as 0. Therefore, it can be concluded that

$$I_{zz}\ddot{\varphi} = M_z = \left(F_{y11}\cos\delta + F_{y12}\cos\delta\right)L_f - L_r\left(F_{y21} + F_{y22}\right) + \left(F_{x11} - F_{x12}\right)\cos\delta\frac{B_f}{2} + \frac{B_r}{2}\left(F_{x21} - F_{x22}\right). \tag{8}$$

$(F_{x11} - F_{x12})\cos\delta(B_f/2) + (B_r/2)(F_{x21} - F_{x22})$ in (8) is the input value of direct yaw moment, so (8) can be converted into

$$M_{\text{yaw\_des}} = \left(F_{x11} - F_{x12}\right)\cos\delta\frac{B_f}{2} + \frac{B_r}{2}\left(F_{x21} - F_{x22}\right), \tag{9}$$

where $M_{\text{yaw\_des}}$ is the direct yaw moment input value when the vehicle is about to lose stability.

DYC adopts sliding mode control algorithm. The law of convergence is exponential:

$$\dot{s} = -\varepsilon\text{sgn}(s) - k_s s \quad \varepsilon > 0, k_s > 0, \tag{10}$$

where ε and k_s are adjustable parameters to eliminate chattering.

In this paper, the yaw rate and sideslip angle of mass center are taken as control variables. The sliding surface s can be expressed as

$$s = \dot{\varphi} - \dot{\varphi}_{\text{nom}} + \xi\left(\beta - \beta_{\text{nom}}\right), \tag{11}$$

where ξ is an adjustable parameter.

For the differential of sliding surface s, the following results can be obtained:

$$\dot{s} = \ddot{\varphi} - \ddot{\varphi}_{\text{nom}} + \xi\left(\dot{\beta} - \dot{\beta}_{\text{nom}}\right). \tag{12}$$

After combining formulas (9), (11), and (12), the direct yaw moment required by the vehicle to maintain the lateral stability under the limit condition is as follows:

$$M_{\text{yaw\_des}} = I_{zz}\left[\dot{\varphi}_{\text{nom}} - \xi\left(\dot{\beta} - \dot{\beta}_{\text{nom}}\right) - \varepsilon\text{sgn}(s) - k_s s\right] - \left[\left(F_{y11}\cos\delta + F_{y12}\cos\delta\right)L_f - L_r\left(F_{y21} + F_{y22}\right)\right]. \tag{13}$$

4. Engine Torque Control Algorithm

Engine control (engine torque control, ETC) is implemented on the basis of the traction system control TCS. When ETC intervenes, the engine torque adjustment value will be transmitted to the engine management system (EMS) via the CAN bus. EMS makes corresponding adjustments according

to the engine torque adjustment value. The engine control architecture is shown in Figure 5. The mathematical expression of engine output torque is

$$T_e = T_{\text{base}} - \Delta T_{\omega e} - T_{\text{fast}}, \tag{14}$$

where T_{base} is the basic value of engine output torque (T_{base} is obtained by looking up the MAP table according to the current throttle opening parameters and engine speed parameters); T_{fast} is the target value of engine torque reduction after ETC intervention; and $\Delta T_{\omega e}$ is the engine torque correction parameter, and its mathematical model can be expressed as follows [33]:

$$\Delta T_{\omega e} = J_e \frac{\mathrm{d}\omega_e}{\mathrm{d}t} \cdot \lambda\left(\frac{\mathrm{d}\omega_e}{\mathrm{d}t}\right), \tag{15}$$

where J_e is the crankshaft moment of inertia parameter; $\lambda(\mathrm{d}\omega_e/\mathrm{d}t)$ is the dynamic compensation factor of engine speed; and ω_e is the engine speed. It can be seen that the correction value $\Delta T_{\omega e}$ is closely related to the engine speed [33].

4.1. Engine Torque Regulation Algorithm Based on Variable Parameter PID. The wheel speed of the car wheel is selected as the control variable. Because wheel speed and slip ratio constitute a mathematical relationship, wheel speed can be obtained by the wheel speed sensor. As a control variable, the target value of wheel speed is

$$v_{\text{nom}} = \frac{v_{\text{ref}}}{(1 - \lambda_{\text{nom}})}, \tag{16}$$

where $\lambda_{\text{nom}} = f(\lambda_p) \cdot K_{\text{TCS\_flag}} + \lambda_{\text{corr}}$; v_{ref} is the reference speed of the vehicle; $K_{\text{TCS\_flag}}$ is the flag of TCS control intervention, which is set to 1 when the wheel slip rate exceeds the TCS threshold value and set to zero if it does not exceed it; λ_{corr} is the correction parameter of the slip rate during ETC intervention, and the calculation of this value is the key of ETC algorithm, which is introduced in Section 4.2; and $f(\lambda_p)$ is the optimal slip rate of the wheel under the current driving condition during TCS intervention, and the calculation can be found in [31].

ETC adopts PID control algorithm with variable parameters. The algorithm formula can be expressed as follows:

$$\begin{cases} T_{\text{fast}} = K_P \mu_{\text{corr}} \Delta v + K_I \mu_{\text{corr}} (\Delta v_k - \Delta v_{k-1}) + K_D \mu_{\text{corr}} \int \Delta v \mathrm{d}t, \\ \Delta v = v_T - v_{\text{nom}}, \end{cases} \tag{17}$$

where v_T is the average speed of the two wheels connected to the drive shaft. The ranges of three parameters K_P, K_I, and K_D are shown in Table 2. The range of μ_{corr} is shown in Figure 6.

4.2. Target Value Calculation Process of Engine Torque Regulation. λ_{corr} is calculated by fuzzy algorithm. The calculation architecture of λ_{corr} is shown in Figure 7.

Table 2: Parameter table of variable parameter PID.

μ	K_P	K_I	K_D
$\Delta v > E_2$	111	102	6
$E_1 < \Delta v \le E_2$	222	210	10
$0 < \Delta v \le E_1$	196	122	70

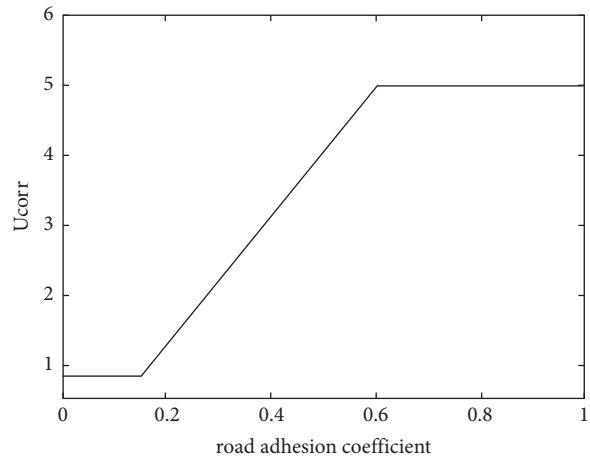

Figure 6: Relationship between adhesion coefficient and μ_{corr}.

The input variable of fuzzy algorithm 1 is $|e(\dot{\varphi})| = |\dot{\varphi} - \dot{\varphi}_{\text{nom}}|$. When the vehicle is in a stable state in the steering process, its yaw rate will follow its target value. The target yaw angle can be calculated according to the linear two-degree-of-freedom vehicle model [24]. When the input variable 1 is not equal to 0, it means that the current state of the car is understeer or oversteer. The range of the input variable is [0,1]. 0 means that the car is in a stable state when steering, and 1 means that the car is under steering or over steering, which is very serious. At this time, ETC controller needs to reduce the engine output torque to improve the vehicle state. The fuzzy set of input variable 1 is shown in Figure 8.

The second input variable is $|e(\beta)| = |\beta - \beta_{\text{nom}}|$, and its range is [0,1]. 0 means that the car is in a stable state. 1 means that the car deviates greatly from the target trajectory during the steering process. The fuzzy set of input variable 2 is shown in Figure 9.

Input variable 3 is $|\dot{\delta}|$, $|\dot{\delta}|$ is the absolute value of the steering wheel angle change rate, which represents the driver's steering input, and its range is [0,1]. 0 means that the driver's steering wheel input changes constantly during the steering process, and 1 means that the steering wheel angle change rate is too large during the steering process. The fuzziness of input variable 3 is shown in Figure 10.

The output is λ_{corr}, and its range is [0,1]. The fuzzy subset is shown in Figure 11.

5. Simulation Results and Analysis

The simulation platform was jointly constructed by Matlab/Simulink, CarSim, and AMESim software. The joint simulation platform scheme is shown in Figure 12. The control

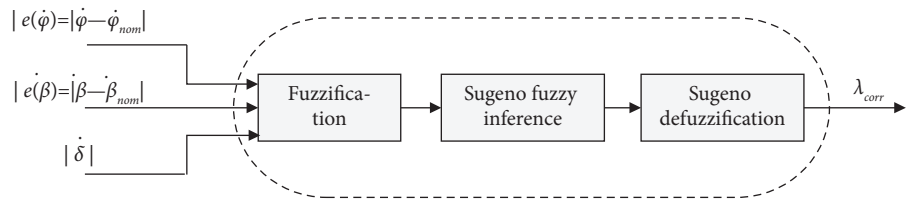

Figure 7: Structure diagram of fuzzy algorithm for λ_{corr}.

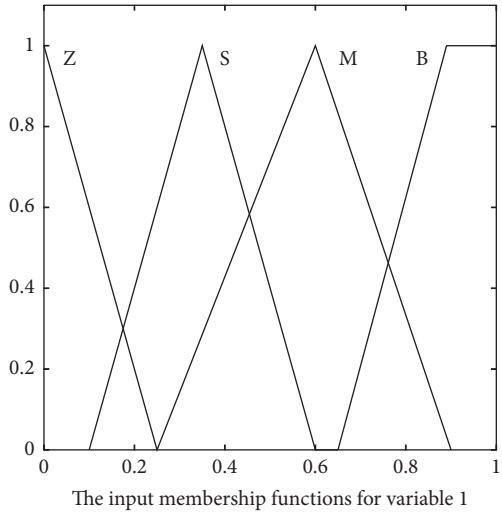

Figure 8: Membership function diagram of input variable 1.

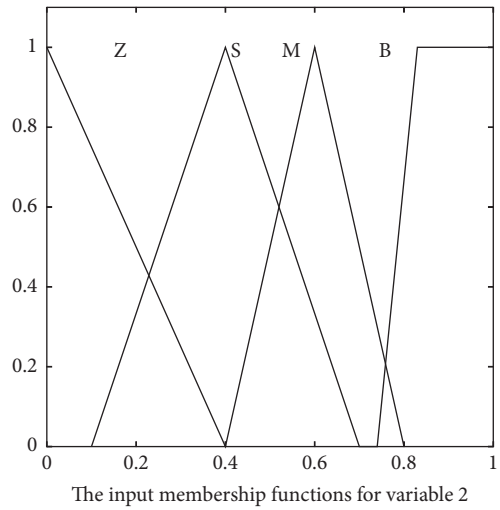

Figure 9: Membership function diagram of input variable 2.

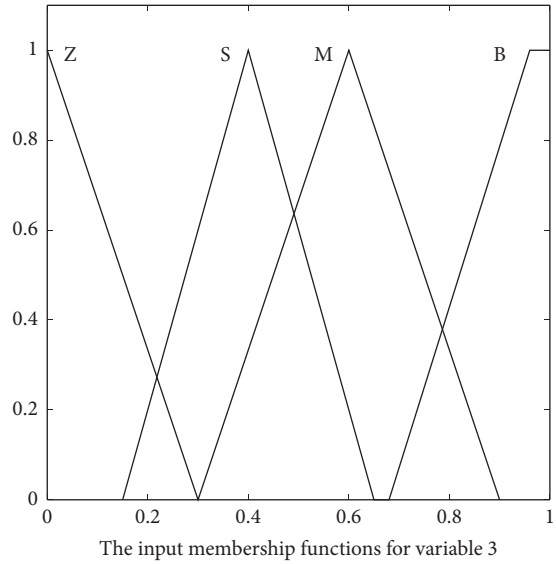

Figure 10: Membership function diagram of input variable 3.

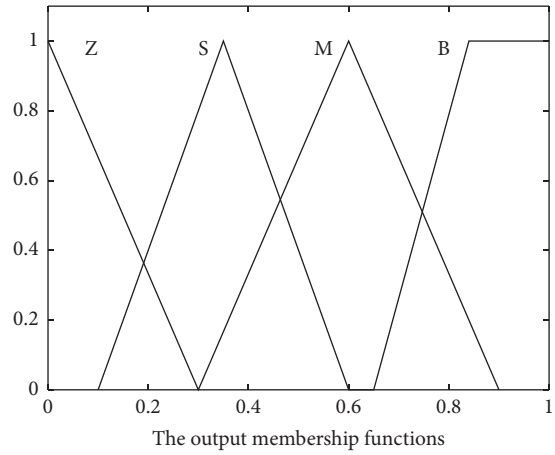

Figure 11: Membership function diagram of output variable.

algorithm of direct yaw moment and engine torque adjustment is programmed by Matlab/Simulink software. The wheel cylinder pressure control and wheel cylinder pressure estimation algorithm modules are implemented according to reference [33]. The hydraulic control unit is modeled using AMESim software. In the algorithm simulation verification part, the sine hysteresis experiment and the steering wheel amplification experiment that comply with the FMVSS126 regulations are used for verification. The vehicle parameters are shown in Table 3.

5.1. Case 1: Sine with Dwell Maneuver. Figure 13 shows a curve with a steering wheel input angle. In the set simulation conditions, the vehicle speed is 80 km/h, and the road adhesion coefficient is 0.9. In the sine hysteresis simulation, data comparison of two experimental conditions was carried

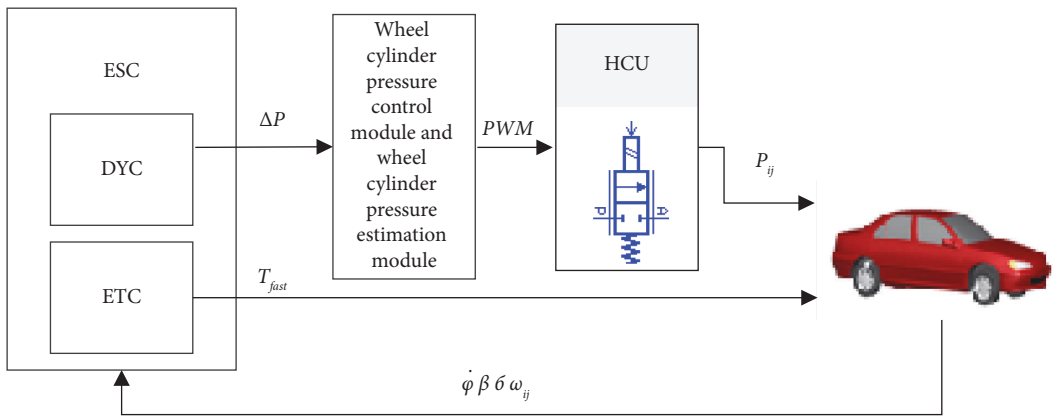

Figure 12: The joint simulation platform scheme.

Table 3: The vehicle parameters.

Parameters	Value
Vehicle mass	1510 kg
m_{usf}, m_{usr}	85,95 kg
L_f, L_r	1.105,1.545 m
I_{zz}	2200 kg·m^2
I_{zzx}	325 kg.m^2
R_w	0.336 m
C_{y1j}, C_{y2j}	15320, 16120 N/rad

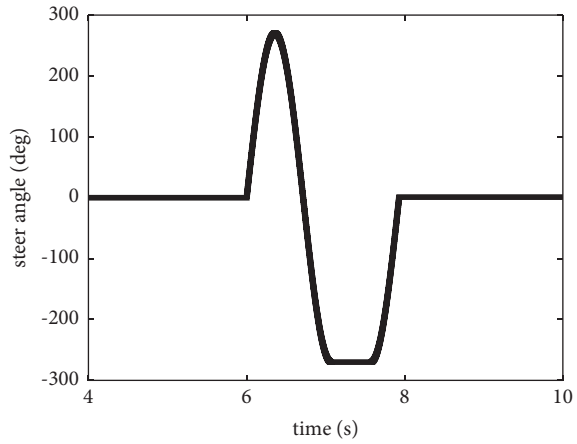

Figure 13: The input angle of steer.

out. One is the experimental result without stability control, and the other is the experimental result with the algorithm proposed in this paper. It can be seen from Figures 14 and 15 that in 7 seconds, the yaw rate and lateral acceleration of the car without control no longer follow the trend of direction change. Therefore, it can be judged that the vehicle without ESC control is completely out of control. For vehicles using the algorithm proposed in this paper, the yaw rate and lateral acceleration closely follow the changes of the steering wheel angle input value. Figure 16 shows the $\beta - \dot{\beta}$ phase plane curve. It can be seen from Figure 16 that the curve convergence degree of the algorithm adopted in this paper is much better than that of uncontrolled vehicles.

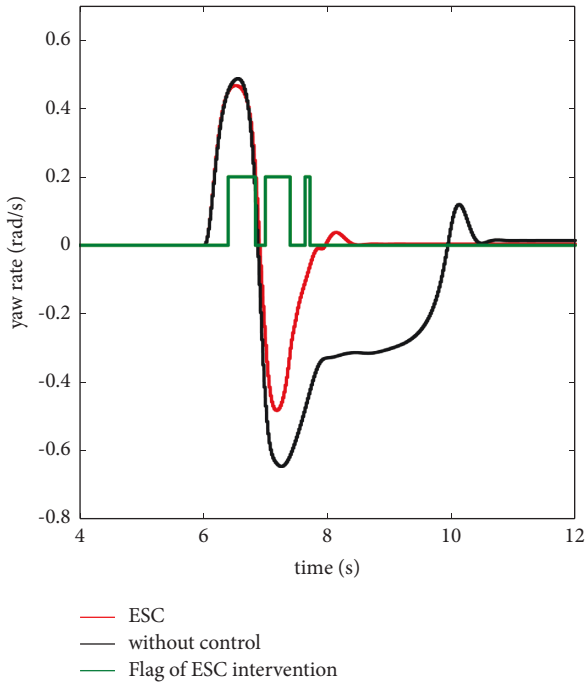

Figure 14: Yaw rate under sine with dwell maneuver.

5.2. Case 2: Steering Wheel Angle Input Increase. The simulation conditions of steering wheel angle input increase are set as follows: when the vehicle is driving at high speed, the driver gradually increases the steering wheel angle to verify whether the vehicle can ensure lateral stability. The input value of steering wheel angle is shown in Figure 17. The speed of the simulated vehicle is 90 km/h. The road is icy and snowy, and the adhesion coefficient is 0.3. Unlike the sine hysteresis experiment, the vehicle maintains a constant speed throughout the experiment. In the test, the driver model needs to control the fuel supply. This simulation test was used to verify the coordinated control effect of direct yaw moment and engine torque adjustment.

The simulation results of the three cases are compared. The first is a vehicle without control, the second is a vehicle that relies solely on direct yaw moment control, and the third is a vehicle that uses DYC and ETC coordinated

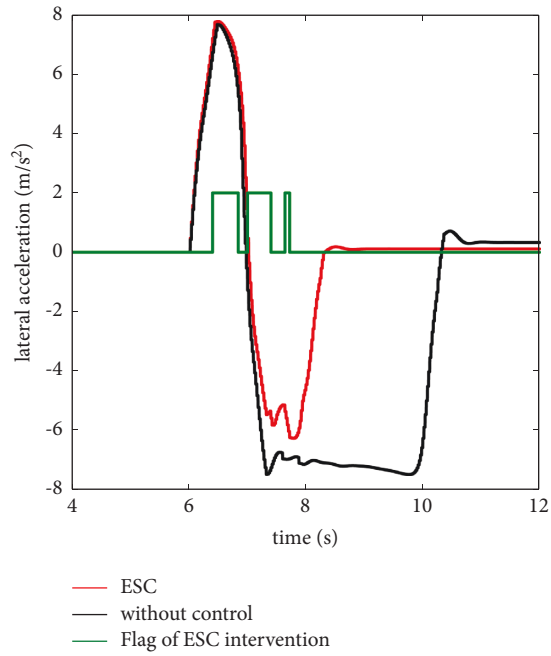

Figure 15: Lateral acceleration under sine with dwell maneuver.

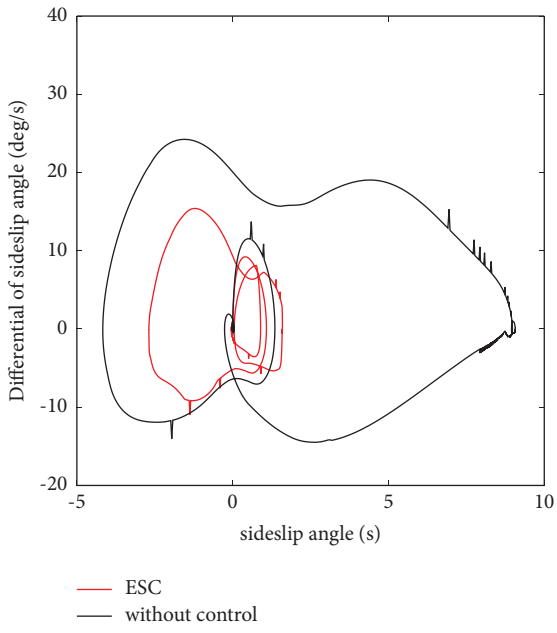

Figure 16: Phase plane under sine with dwell maneuver.

control. Figure 18 shows the curve of the yaw rate. Figure 19 shows the lateral acceleration curve. It can be seen from Figures 18 and 19 that the vehicle without a control algorithm starts to lose control completely at 7 seconds because at this time, the yaw rate and lateral acceleration of the vehicle are no longer consistent with the steering wheel. In the other two cases, the vehicle can maintain the lateral stability of the vehicle. However, in the third case, the yaw rate of the vehicle is closer to the target value. Figure 20 shows the $\beta - \dot{\beta}$ phase plan curve. It can be seen from Figure 20 that the curve convergence degree of the vehicle

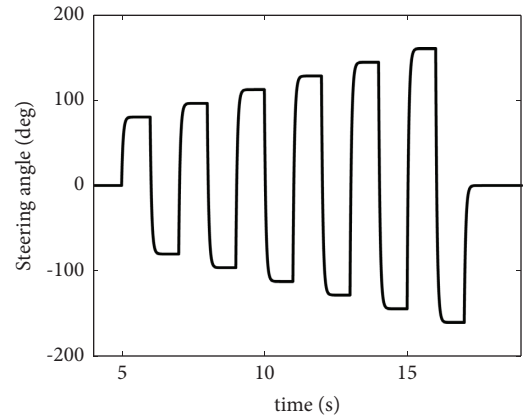

Figure 17: The input angle of steer.

proposed in this paper is better than that of the other two simulation conditions. Under the steering wheel angle input increase condition, the yaw rate and the lateral acceleration change considerably. By using a joint control method, the peak value of the yaw rate for joint control is reduced by 32.19%, compared to the corresponding peak with DYC control, indicating improved stability.

The following performance indicators are defined to objectively evaluate the controllers.

(i) Mean error: $\eta_{\dot{\varphi}} = (1/n)\sum_{i=1}^{n} |\dot{\varphi}_{\text{nom}}(t) - \dot{\varphi}(t)|$.

(ii) Standard deviation: $\sigma_{\dot{\varphi}} = \sqrt{(1/n)\sum_{i=1}^{n} (\dot{\varphi}_{\text{nom}}(t) - \dot{\varphi}(t))^2}$.

The performance indicators in Table 4 highlight the following. (1) Without the intervention of the control algorithm, the yaw rate of the vehicle reached the maximum value in the experiment. This situation is typical of uncontrollable vehicle behavior. (2) Table 4 shows the peak values of yaw rate(Max $|\dot{\varphi}|$) and lateral acceleration(Max $|a_y|$) under three simulation conditions. For the vehicle with DYC and ETC coordinated control, the peak yaw rate and lateral acceleration are the minimum. It shows that DYC and ETC coordinated control algorithm has the best yaw rate tracking performance. (3) For the vehicle with DYC and ETC coordinated control, the mean error $\eta_{\dot{\varphi}}$ and standard error $\sigma_{\dot{\varphi}}$ of the yaw rate are the minimum under the three simulation conditions.

6. Experimental Results

The MG Rui-Teng produced by SAIC Motor Passenger Car was selected as the experimental vehicle. A steering wheel angle sensor, a yaw rate sensor, and a SpeedBox tester are installed on the car. To ensure safety, an anti-roll bar is installed on the car. Figure 21 shows the status of the vehicle modification and the layout of the internal equipment. The actual vehicle test was conducted at the GM-Asia test track. A high-adhesion road with an adhesion coefficient of 0.9 was selected as the experimental road. The double-shifting working condition experiment conforming to ISO3888-1 standard was selected as the experimental working condition. The initial speed of the test vehicle is 75 km/h. The

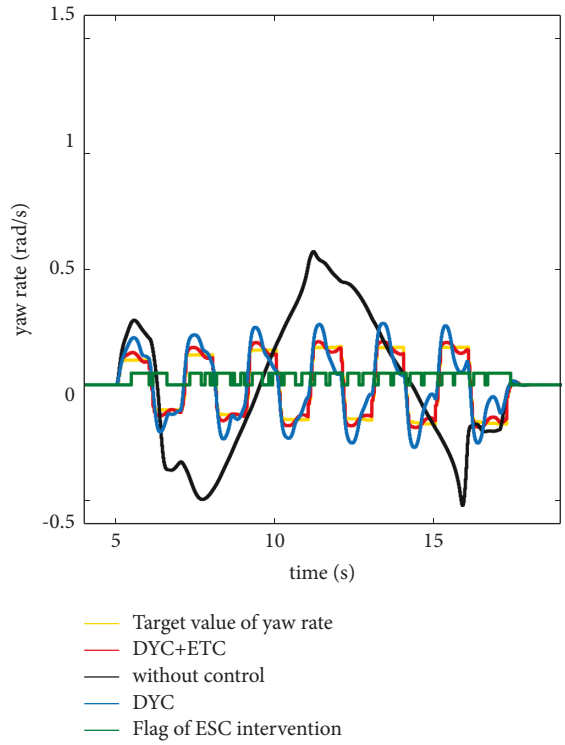

Figure 18: Yaw rate under case 2.

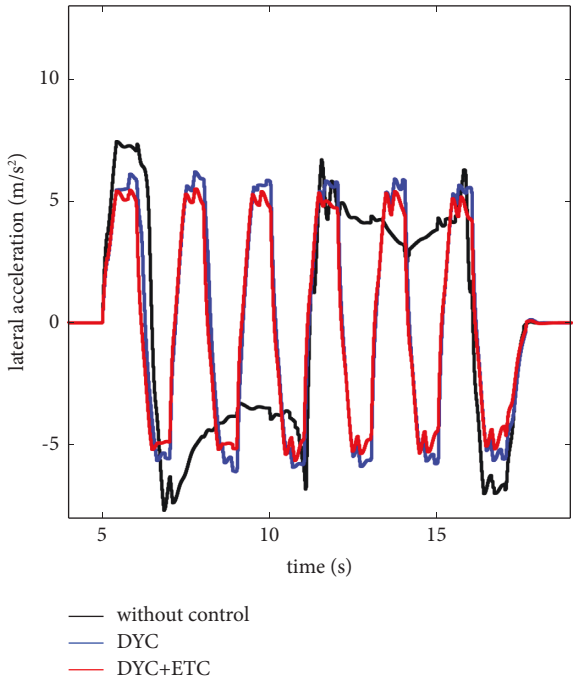

Figure 19: Lateral acceleration under sine with dwell maneuver.

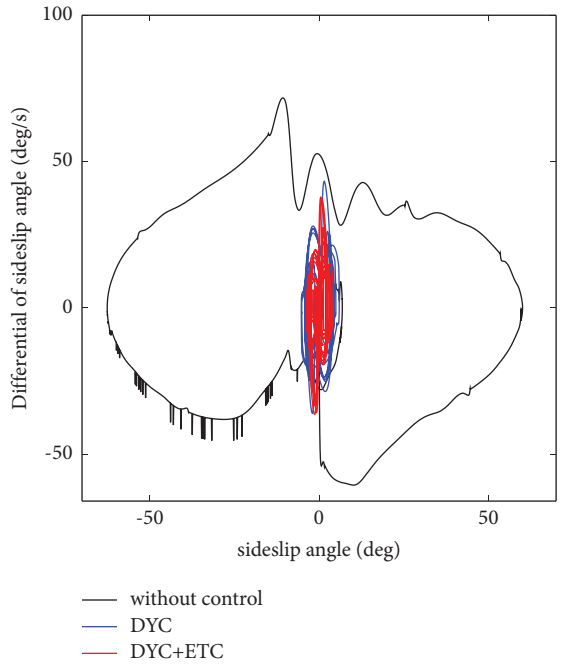

Figure 20: Phase plane under case 2.

Figure 21: The status of the vehicle modification.

Table 4: Performance indicators of the controlled vehicle for the simulation.

	Without control	DYC	DYC + ETC
Mean error	0.35	0.1	0.03
Standard deviation	0.39	0.12	0.04
Max $\lvert\dot{\varphi}\rvert$ (rad/s)	0.51	0.31	0.23
Max $\lvert a_y\rvert$ (m/s^2)	8.01	6.34	5.72

experiment was conducted in two situations. One is to turn off the ESC controller effect verification, and the other is to turn on the ESC controller effect verification.

Figure 22 shows the front wheel angle curve and the lateral acceleration curve of the vehicle without ESC control. It can be seen from Figure 22 that the lateral acceleration reaches its maximum value (8.51 m/s^2) at 4.02 seconds. Lateral acceleration and yaw rate did not closely follow the trend of front wheel angle changes. It shows that the trajectory of the car has deviated from the driver's operation. At this time, the car is already in an unstable state. The double-line shifting experiment without ESC control was done 10 times. In each experiment, the car hit the isolation pile.

Figure 23 shows the front wheel angle and lateral acceleration data of the vehicle with the ESC turned on. It can be seen from Figure 23 that ESC control has played a role in

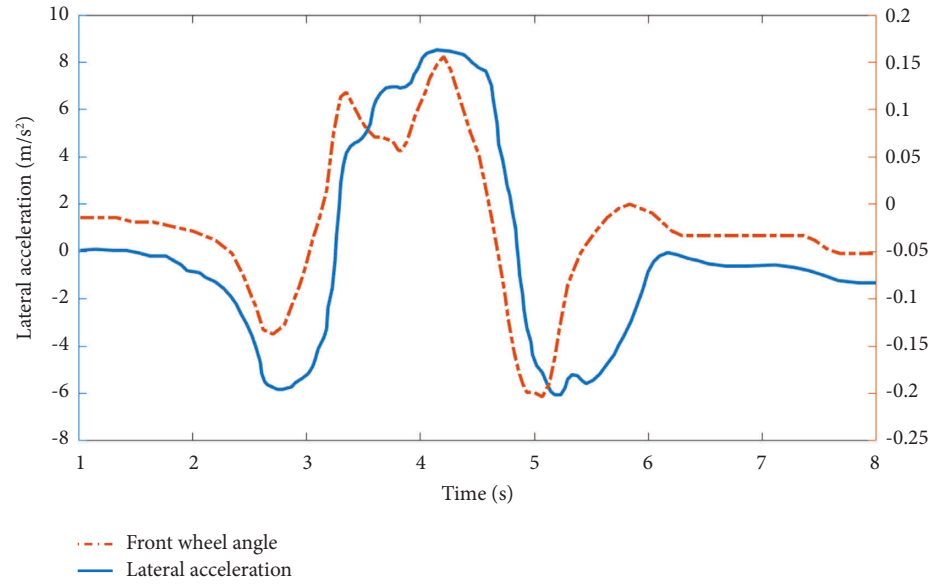

Figure 22: The front wheel angle curve and the lateral acceleration curve of the vehicle without ESC control.

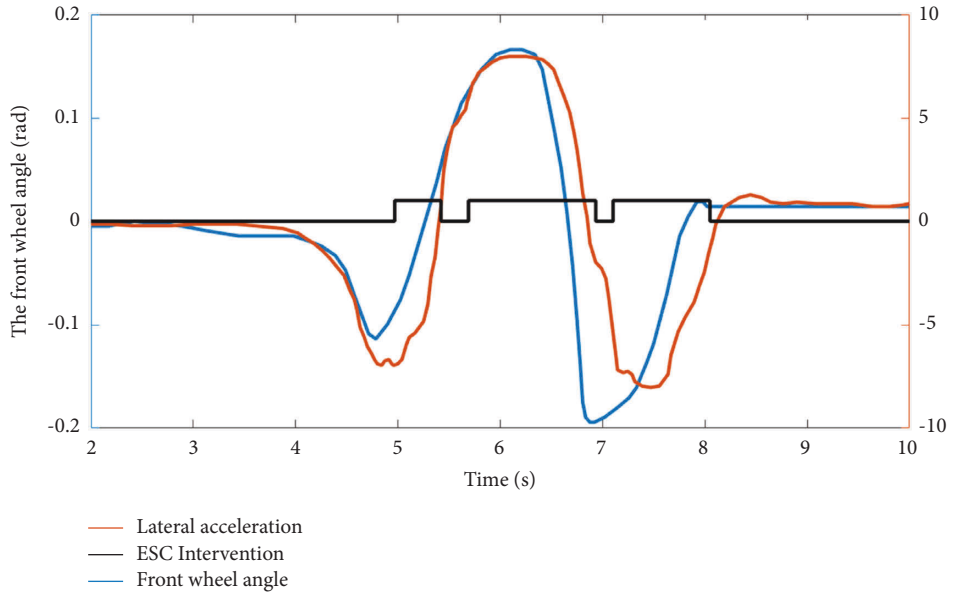

Figure 23: The front wheel angle and lateral acceleration data of the vehicle with the ESC turned on.

improving the stable state of the vehicle at 4.89 s, 5.71 s, and 7.21 s. The change trend of yaw rate and lateral acceleration is basically consistent with the front wheel angle.

7. Conclusion

The vehicle is taken as the research object, mainly studying the stability control system of the vehicle. Vehicle stability control system can improve the lateral stability of the vehicle under extreme conditions. This paper presents a coordinated control algorithm of direct yaw moment and engine torque regulation. Firstly, the DYC intervention timing method and ETC intervention timing method are studied. Then, the direct yaw moment control based on variable structure sliding mode algorithm and ETC algorithm based on fuzzy algorithm are designed. Matlab/Simulink, AMESim, and CarSim are used for joint simulation. The simulation results show that the algorithm can effectively improve the vehicle stability.

The vehicle stability algorithms in this paper are obtained through modern control theory. The algorithm implementation mainly relies on Simulink to establish the algorithm model, and the algorithm is implemented by the controller Autobox. In the next step, we need to consider converting Simulink algorithm model into C code and designing ESC hardware circuit, so as to finally realize the production of ESC.

Data Availability

The data used to support the findings of this study are available from the corresponding author upon request.

Conflicts of Interest

The authors declare that they have no conflicts of interest.

Acknowledgments

This study was supported by the Henan Province Science & Technology Research Project (nos. 212102210046 and 212102311151).

References

[1] H. Y. Li, J. Y. Yu, C. Hilton, and H Liu, "Adaptive sliding-mode control for nonlinear active suspension vehicle systems using T–S fuzzy approach," *IEEE Transactions on Industrial Electronics*, vol. 60, no. 8, pp. 3328–3338, Aug, 2013.

[2] H. Wang, H. Kong, Z. Man, D. M. Tuan, Z. Cao, and W. Shen, "Sliding mode control for steer-by-wire systems with AC motors in road vehicles," *IEEE Transactions on Industrial Electronics*, vol. 61, no. 3, pp. 1596–1611, 2014.

[3] X. peng, H. zhe, G. Guifang, X. Gang, C. Binggang, and L. Zengliang, "Driving and control of torque for direct-wheel-driven electric vehicle with motors in serial," *Expert Systems with Applications*, vol. 38, no. 1, pp. 80–86, Jan. 2011.

[4] T. Yoshioka, T. Adachi, T. Butsuen, H. Okazakic, and H. Mochizukid, "Application of sliding-mode theory to direct yaw-moment control," *JSAE Review*, vol. 20, no. 4, pp. 523–529, Oct. 1999.

[5] X. Yang, Z. Cai, T. Jin, Z. Tang, and S. Gao, "A three-phase search approach with dynamic population size for solving the maximally diverse grouping problem," *European Journal of Operational Research*, vol. 302, no. 3, pp. 925–953, 2022.

[6] J. Wang, Q. Wang, L. Jin, and C. Song, "Independent wheel torque control of 4WD electric vehicle for differentialdrive assisted steering," *Mechatronics*, vol. 21, no. 1, pp. 63–76, Feb. 2011.

[7] S. Ding and J. Sun, "Direct yaw-moment control for 4WID electric vehicle via finite-time control technique," *Nonlinear Dynamics*, vol. 88, no. 1, pp. 239–254, 2017.

[8] F. Tahami, S. Farhangi, and R. Kazemi, "A fuzzy logic direct yaw-moment control system for all-wheel-drive electric vehicles," *Vehicle System Dynamics*, vol. 41, no. 3, pp. 203–221, Apr. 2004.

[9] E. Esmailzadeh, A. Goodarzi, and G. R. Vossoughi, "Optimal yaw moment control law for improved vehicle handling," *Mechatronics*, vol. 13, no. 7, pp. 659–675, Sep. 2003.

[10] M. Doumiati, O. Sename, L. Dugard, J. J. Martinez-Molina, P. Gaspar, and Z. Szabo, "Integrated vehicle dynamics control via coordination of active front steering and rear braking," *European Journal of Control*, vol. 19, no. 2, pp. 121–143, Mar. 2013.

[11] H. Li, X. Jing, and H. R. Karimi, "Output-feedback-based H_{∞} control for vehicle suspension systems with control delay," *IEEE Transactions on Industrial Electronics*, vol. 61, no. 1, pp. 436–446, Jan. 2014.

[12] B. Li, J. Xu, T. Jin, and Y Shu, "Piecewise parameterization for multifactor uncertain system and uncertain inventory-promotion optimization," *Knowledge-Based Systems*, vol. 255, Article ID 109683, 2022.

[13] T. Jin, S. Gao, H. Xia, and H Ding, "Reliability analysis for the fractional-order circuit system subject to the uncertain random fractional-order model with Caputo type," *Journal of Advanced Research*, vol. 32, pp. 15–26, 2021.

[14] T. Jin, X. Yang, H. Xia, and H. Ding, "Reliability index and option pricing formulas of the first-hitting time model based on the uncertain fractional-order differential equation with Caputo type," *Fractals*, vol. 29, no. 01, Article ID 2150012, 2021.

[15] T. Jin, H. Xia, and S. Gao, "Reliability analysis of the uncertain fractional order dynamic system with state constraint," *Mathematical Methods in the Applied Sciences*, vol. 45, no. 5, pp. 2615–2637, 2022.

[16] T. Kawabe, M. Nakazawa, I. Notsu, and Y. Watanabe, "A sliding mode controller for wheel slip ratio control system," *Vehicle System Dynamics*, vol. 26, no. 2, pp. 117–126, 1996.

[17] L. Liu, S. Ding, and X. Yu, "Second-order sliding mode control design subject to an asymmetric output constraint," *IEEE Transactions on Circuits and Systems II: Express Briefs*, vol. 68, no. 4, pp. 1278–1282, 2021.

[18] Q. Hou, S. Ding, and X. Yu, "Composite super-twisting sliding mode control design for PMSM speed regulation problem based on a novel disturbance observer," *IEEE Transactions on Energy Conversion*, vol. 36, no. 4, pp. 2591–2599, 2021.

[19] S. Ding, W. H. Chen, K. Mei, and D. J. Murray-Smith, "Disturbance observer design for nonlinear systems represented by input-output models," *IEEE Transactions on Industrial Electronics*, vol. 67, no. 2, pp. 1222–1232, 2020.

[20] H. Du, C. Jiang, G. Wen, W. Zhu, and Y. Cheng, "Current sharing control for parallel DC-DC Buck converters based on finite-time control technique," *IEEE Transactions on Industrial Informatics*, vol. 15, no. 4, pp. 2186–2198, 2019.

[21] Q. Meng, T. Zhao, C. Qian, Z. y. Sun, and P. Ge, "Integrated stability control of AFS and DYC for electric vehicle based on non-smooth control," *International Journal of Systems Science*, vol. 49, no. 7, pp. 1518–1528, 2018.

[22] M. Akar and J. C. Kalkkuhl, "Lateral dynamics emulation via a four-wheel steering vehicle," *Vehicle System Dynamics*, vol. 46, no. 9, pp. 803–829, 2008.

[23] S. Ding, L. Liu, and W. X. Zheng, "Sliding mode direct yaw-moment control design for in-wheel electric vehicles," *IEEE Transactions on Industrial Electronics*, vol. 64, no. 8, pp. 6752–6762, 2017.

[24] H. Shraim, M. Ouladsine, L. Fridman, and M. Romero, "Vehicle parameter estimation and stability enhancement using sliding modes techniques," *International Journal of Vehicle Design*, vol. 48, no. 3/4, pp. 230–254, Apr. 2008.

[25] F. Borrelli, A. Bemporad, M. Fodor, and D Hrovat, "An MPC/hybrid system approach to traction control," *IEEE Transactions on Control Systems Technology*, vol. 14, no. 3, pp. 541–552, 2006.

[26] H. Lee and M. Tomizuka, "Adaptive vehicle traction force control for intelligent vehicle highway systems[J]," *IEEE Transactions on Industrial Electronics*, vol. 50, no. 1, pp. 37–47, 2003.

[27] S. Inagaki, L. Kushiro, and M. Yamamoto, "Analysis on Vehicle Stability in Critical Cornering Using Phase-Plane Method," *Jsae Review*, vol. 2, 1995.

[28] C. Zhang, X. QS, and Le He, "A study on the influence of sideslip angle at mass center on vehicle stability," *Automotive Engineering*, vol. 33, no. 4, pp. 5–10, 2011.

[29] J. Liu, J. Song, H. Li, and H Huang, "Direct yaw-moment control of vehicles based on phase plane analysis," *Proceedings of the Institution of Mechanical Engineers - Part D: Journal of*

Automobile Engineering, vol. 236, no. 10-11, pp. 2459–2474, 2022.

[30] W. Liu, L. Xiong, B. Leng, and M Haolan, *Vehicle Stability Criterion Research Based on Phase Plane method*, SAE Technical Paper, 2017.

[31] J. Yoon, W. Cho, J. Kang, B. Koo, and K Yi, "Design and evaluation of a unified chassis control system for rollover prevention and vehicle stability improvement on a virtual test track," *Control Engineering Practice*, vol. 18, no. 6, pp. 585–597, 2010.

[32] J. Chen, J. Song, L. I. Liang, and X Ran, "A novel pre-control method of vehicle dynamics stability based on critical stable velocity during transient steering maneuvering," *Chninese Journal of Mechanical Engineering*, vol. 29, no. 3, pp. 475–485, 2016.

[33] M. Kang, L. Li, H. Li, J. Song, and Z Han, "Coordinated vehicle traction control based on engine torque and brake pressure under complicated road conditions," *Vehicle System Dynamics*, vol. 50, no. 9, pp. 1473–1494, 2012.